ISSN 1391-0256

Journal of the Sri Lanka Association for the Advancement of Science

Volume 8 Issue 1, 2026

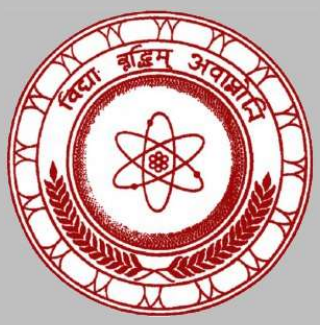

JSLAAS

Founded in 1944 and incorporated by the Act of Parliament No 11 of 1966

Journal of the Sri Lanka Association for the Advancement of Science is a biannual publication. Selected research work from annual research sessions (based on scientific merit) as well as other research articles are invited to submit research manuscripts as per the guidelines provided by SLAAS. SLAAS members may also separately submit their papers for publication. The Journal can be accessed on-line to view and download the full text of the articles published respective to the volumes free of charge

Submission Manuscript

Only online submission, Web: https://journal.slaas.lk,e-ISSN: 2682-6992

Members of the Editorial Board

Exchanges: Please address all requests to the Secretary, *Sri Lanka Association for the Advancement of Science, "Vidya Mandiraya" 120/10, Wijerama Mawatha Colombo 07, Sri Lanka*

Table of Contents

Controlled Sulfur Incorporation in SILAR-Deposited CdS Quantum Dots for Suppression of Interfacial Recombination in TiO_2 Quantum Dot-Sensitized Solar Cells

N.F. Ajward*, J.V.P. Fernando and V.P.S. Perera

Department of Physics, The Open University of Sri Lanka, Nawala, Nugegoda

ABSTRACT

Quantum dot-sensitized solar cells (QDSSCs) are limited by severe interfacial recombination and inefficient electron transport at the TiO_2/CdS junction. In this work, the interfacial charge dynamics were controlled by regulating sulfur availability during successive ionic layer adsorption and reaction (SILAR) growth of CdS quantum dots on mesoporous TiO_2 photoanodes. Sulfur was introduced in controlled molar ratios relative to the Cd^{2+} precursor to modify defect density and band alignment.

An optimum sulfur level produced a marked improvement in photovoltaic performance, where power conversion efficiency increased from 0.262% (undoped CdS) to 0.519%, accompanied by higher photocurrent density and open-circuit voltage. Electrochemical impedance analysis showed a strong increase in recombination resistance and a prolonged electron lifetime (0.017 s → 0.159 s), while Mott–Schottky measurements revealed a positive flat-band shift (−0.747 V → −0.588 V vs Ag/AgCl), indicating improved interfacial energetics. The enhancement originates from sulfur-induced passivation of surface trap states in CdS, which suppresses back electron transfer to the electrolyte and facilitates forward electron transport through the TiO_2 network. Consequently, performance enhancement is dominated by interfacial recombination suppression.

These results demonstrate that tuning sulfur incorporation during CdS growth provides a simple and scalable strategy to engineer interfacial charge transport and improve the efficiency and stability of TiO_2/CdS QDSSCs.

Keywords: Quantum Dot-Sensitized Solar Cells (QDSSCs), Sulfur Doping, Cadmium Sulfide, SILAR, Photovoltaic Performance

---

* nf2010.ajward@gmail.com

INTRODUCTION

The increasing demand for sustainable energy has intensified research on low-cost, high-efficiency photovoltaic technologies. Among emerging systems, dye-sensitized and quantum dot-sensitized solar cells (DSSCs and QDSSCs) have attracted considerable attention due to their broad spectral response, tunable optical properties, and simple fabrication processes (Grätzel, M., 2001; Nozik, A. J., 2002). In particular, QDSSCs offer advantages such as high extinction coefficients and size-dependent electronic structures, enabling the possibility of exceeding conventional efficiency limits through mechanisms including multiple exciton generation (MEG) (Klimov, V. I., 2006; Shockley & Queisser, 1961).

The electron transport layer (ETL) plays a critical role in charge separation and collection in these devices. Titanium dioxide (TiO_2) remains the most widely used ETL owing to its wide band gap (~3.2

eV), chemical stability, and favorable electron mobility (O'Regan, B., & Grätzel, M., 1991; Wang, P. etl., 2003). Its mesoporous structure provides a large surface area for quantum dot loading, improving light absorption (Bisquert, J. et al., 2004). However, TiO_2 suffers from limited conductivity and imperfect band alignment with sensitizers, leading to recombination losses and motivating various modification strategies such as doping and surface treatment (Chen & Mao, 2007).

Cadmium-based quantum dots, particularly CdS and CdSe, are widely employed sensitizers because of their strong visible-light absorption and efficient electron injection into TiO_2 (Kamat, P. V., 2008; Hodes, G., 2008). CdS (band gap ≈ 2.4 eV) forms a well-matched heterojunction with TiO_2 and is commonly deposited using chemical bath deposition or the successive ionic layer adsorption and reaction (SILAR) method, allowing controlled growth and interfacial coupling (Lee, H. J. et al., 2009; Santra & Kamat, 2012). Nevertheless, trap-assisted recombination and interfacial defects remain major limitations to device performance.

Sulfur incorporation has been proposed as a strategy to passivate defects, improve band alignment, and enhance carrier transport in CdS systems (Lu, H., et al., 2014). However, the effect of controlled sulfur availability during SILAR growth on recombination dynamics and electron lifetime in TiO_2/CdS QDSSCs remains insufficiently understood. In particular, the relationship between sulfur concentration, charge transport resistance, and flat-band potential has not been systematically investigated.

In this work, CdS quantum dots were grown on TiO_2 photoanodes with controlled sulfur incorporation, and their structural, electronic, and photovoltaic properties were analyzed using electrochemical and spectroscopic techniques. Establishing this relationship provides insight into interfacial charge regulation and offers a practical approach for improving the efficiency and scalability of QDSSCs. The novelty of this study lies in regulating sulfur availability during the SILAR growth of CdS quantum dots and correlating the resulting device performance with recombination resistance, electron lifetime, and flat-band potential. Unlike previous studies that mainly focus on CdS loading, sensitization cycles, or deposition time, this work emphasizes sulfur-mediated interfacial recombination control in TiO_2/CdS QDSSCs.

METHODOLOGY

3.1 Preparation of TiO_2 Plates

TiO_2 paste was prepared by mixing 0.25 g of TiO_2 with 1 ml of 0.1 M HNO_3, one drop of Triton X-100, and one drop of PEG1000, followed by grinding the mixture for 30 minutes using a mortar and pestle. The paste was then applied to pre-cleaned conducting tin oxide (CTO) glass plates (1.0 cm × 2.0 cm) using the doctor blade method. The CTO plates were cleaned in an ultrasonic bath with detergent and distilled water to ensure surface purity. After coating, the TiO_2 films were dried on a hot plate and sintered in a furnace at 450 °C for 45 minutes to achieve the desired properties.

3.2 Preparation of Na_2S and $CdCl_2$ Solutions in Various Concentration

The experiment involved accurately measuring 10.065 g of $CdCl_2$ and 3.902 g of Na_2S using an electronic balance with a precision of ±0.001 g. These compounds were dissolved in 100 mL of distilled water to prepare a 0.5 M solution of Cd^{2+} and S^{2-} ions and the pH of the solution was

adjusted to the optimal value of 4.5 by adding 0.01 M NaOH and 0.01 M HCl solutions dropwise, with continuous monitoring to achieve the desired pH (Hodes, G., 2008).

3.3 Preparation of Na_2S solution with S

Sulfur (S) was added in various amounts to a 0.5M Na_2S solution, as specified in the table, and the mixture was stirred for up to 1 hour. This prepared solution was then used in the successive ionic layer adsorption and reaction (SILAR) method to coat CdS on TiO_2 plates.

Table 1: Mass (in grams) of Sulfur in Samples S1 to S7

Sample number	S1	S2	S3	S4	S5	S6	S7
Mass(g)±0.001 g	0.0176	0.0352	0.0705	0.1410	0.2115	0.2820	0

3.4 Deposition of CdS using SLILAR method.

The SILAR technique was utilized to deposit CdS films onto TiO_2 photoanodes. Each immersion in $CdCl_2$ and Na_2S solutions was maintained for one minute. Following each immersion, the photoanodes were rinsed with distilled water to eliminate excess reagents and then air-dried. To achieve uniform film deposition, the photoanodes were alternately immersed in the complementary precursor solution (cationic or anionic), followed by rinsing. This process was repeated ten times to form a multilayer CdS film. Finally, the coated photoanodes were heated at 80°C on a hot plate for 30 minutes to improve the film's adhesion and crystallinity on the substrate.

3.5 Preparation of Electrolyte

In preparation of 2 ml of electrolyte, 0.130 g of Na_2S, 0.128 g of sulfur, and 0.030 g of KCl were dissolved in a solvent mixture comprising 1.4 ml of methanol and 0.6 ml of distilled water. The solution was stirred for 3 hours using a magnetic stirrer to achieve complete dissolution of the salts. Adjustments to the stirring time may be necessary to prevent sulfur precipitation.

3.6 Fabrication of the cell

A counter electrode with a conductive side positioned directly on the CdS-coated TiO_2 film and held in place using clamps. The space between the electrodes was filled with the prepared electrolyte solution, completing the assembly of the Quantum Dot Sensitized Solar Cell.

3.7 Characterization

The fabricated QDSSCs characterized using a VK-PA-100 PV Power Analyzer to obtain J-V curves, enabling the extraction of critical performance metrics such as Photo Conversion Efficiency (PCE), Photo Current Density (Jsc), Photo Voltage (Voc), and Fill Factor (FF). To ensure reproducibility, at least five devices per batch were tested.

Electrochemical Impedance Spectroscopy (EIS) was employed using a frequency response analyzer (Auto-Lab Nova 2.1) to study the charge transport and recombination processes within the CdS QDSSCs. Impedance spectra measured over a frequency range of 0.1 Hz to 1 MHz under constant simulated light intensity at room temperature, providing insights into interfacial charge transfer resistance and recombination dynamics. These findings are vital for optimizing the QDSSC performance.

Incident Photon-to-Current Efficiency (IPCE) measurements will assess the light-harvesting efficiency of the QDSSCs across the solar spectrum. The effectiveness of the quantum dots in capturing sunlight and converting it into photocurrent will be evaluated using a VK-IPCE-10 system.

RESULTS AND DISCUSSION

4.1 Structural and morphological analysis

4.1.1. Morphology of TiO_2 and TiO_2/CdS

Figure 1 shows the scanning electron microscopy (SEM) images of TiO_2, TiO_2/CdS, and sulfur-treated TiO_2/CdS photoanodes at 100,000× magnification. All samples exhibit a porous nanoparticulate morphology typical of doctor-bladed TiO_2 films. After SILAR treatment, slight surface densification and particle aggregation are observed in the TiO_2/CdS and sulfur-treated TiO_2/CdS samples compared with bare TiO_2.

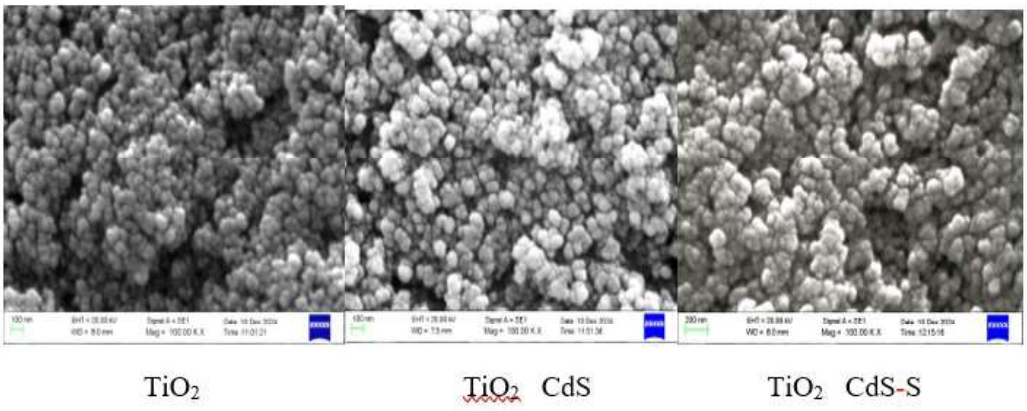

Figure 1: SEM images of TiO_2, TiO_2/CdS and TiO_2/CdS-S

However, these morphological differences are not sufficiently distinct to conclusively confirm CdS deposition or sulfur incorporation from SEM images alone. Therefore, SEM is used here only to compare surface morphology, while direct confirmation of Cd and S distribution would require elemental analysis such as SEM–EDS (Li, W., et al., 2018).

4.1.2 XRD

The XRD patterns are dominated by diffraction peaks corresponding to anatase TiO_2. The main TiO_2 peaks observed at 25.3°, 37.8°, 48.0°, 53.9°, 55.1°, 62.7°, and 75.1° can be assigned to the (101), (004), (200), (105), (211), (204), and (215) planes of anatase TiO_2 (JCPDS No. 21-1272). In the TiO_2/CdS and sulfur-treated TiO_2/CdS samples, distinct CdS-related peaks are weak or not clearly separated from the dominant TiO_2 background. This may be due to low CdS loading, nanoscale crystallite size, overlap between TiO_2 and CdS reflections, or the partially amorphous nature of SILAR-deposited CdS. Therefore, the XRD results are interpreted as supporting structural information rather than conclusive confirmation of crystalline CdS formation or sulfur incorporation.

The weak or unresolved CdS-related features also limit reliable crystallite size estimation for CdS using the Scherrer equation. Therefore, crystallite size calculation was not performed for the CdS phase in the thin-film samples. More accurate crystallite size and phase analysis would require powder samples or thicker films followed by proper annealing under an inert atmosphere (Li, W., et al., 2018).

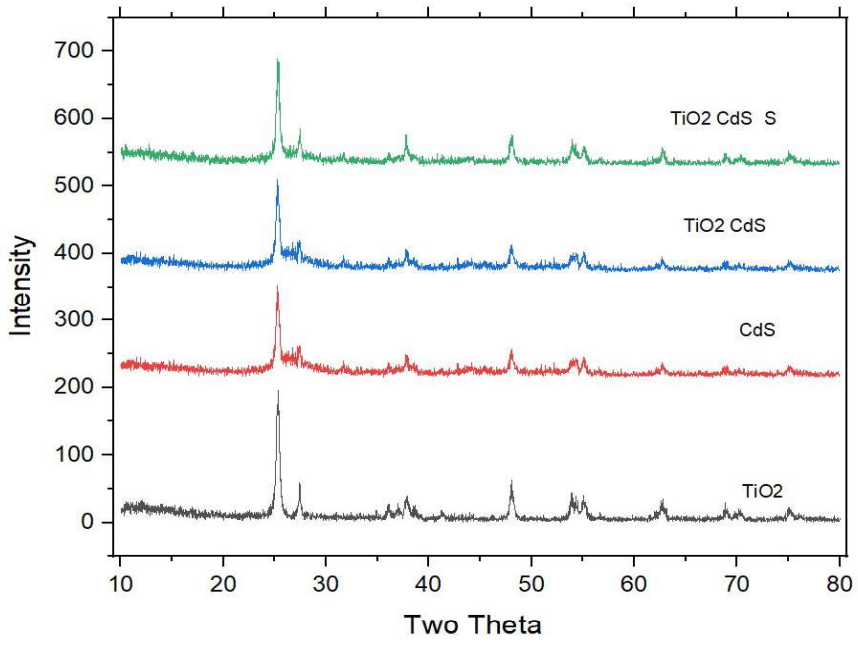

Figure 2: X-ray diffraction (XRD) patterns of TiO_2, CdS, TiO_2/CdS, and TiO_2/CdS with added sulfur (S).

4.1.3 FTIR

FTIR spectroscopy was used to examine surface functional groups and possible chemical changes after CdS deposition and sulfur treatment. Figure 3 presents the FTIR spectra of TiO_2, TiO_2/CdS, and sulfur-treated TiO_2/CdS photoanodes.

The FTIR spectra of TiO_2, TiO_2/CdS, and sulfur-treated TiO_2/CdS show broad absorption bands around 3400 cm^{-1} and 1600 cm^{-1}, which are attributed to O–H stretching and bending vibrations of adsorbed water or surface hydroxyl groups. The strong intensity of these bands indicates that residual moisture may still be present in the samples. Therefore, the FTIR results should be interpreted with caution. Although weak variations are observed in the lower wavenumber region, these changes are not sufficient to conclusively prove CdS formation or sulfur incorporation. Further FTIR measurements after complete drying of the samples are required for more reliable functional group analysis. Thus, the FTIR results are treated as supporting evidence for possible surface modification, while the influence of sulfur treatment is mainly evaluated using the photovoltaic, EIS, and Mott–Schottky results.

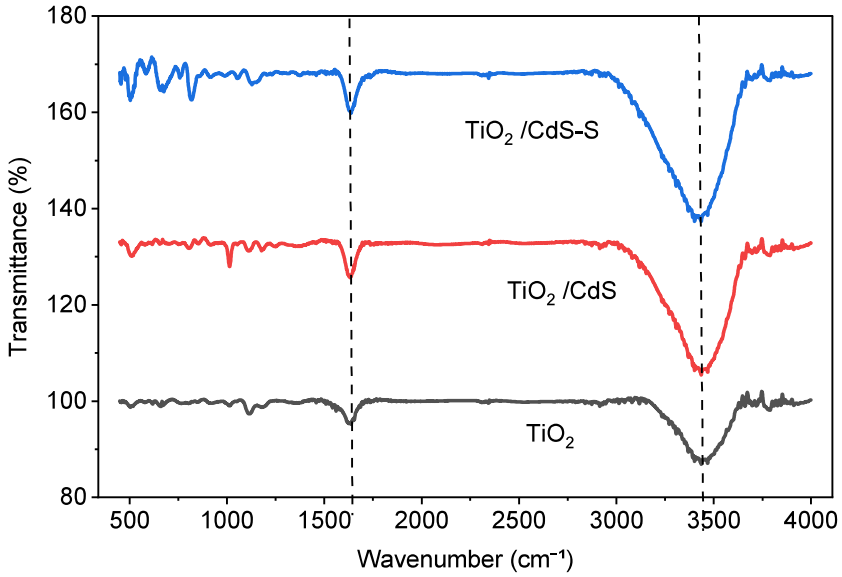

Figure 3: FTIR spectra of TiO_2, TiO_2/CdS, and sulfur-added TiO_2/CdS.

The SEM, XRD, and FTIR results show only subtle changes among TiO_2, TiO_2/CdS, and sulfur-treated TiO_2/CdS samples. This may be due to low CdS loading, nanoscale or partially amorphous CdS formation, and the dominance of the TiO_2 matrix in the structural spectra. Therefore, these techniques are considered supportive rather than conclusive evidence for CdS and sulfur incorporation. The influence of sulfur treatment is mainly supported by the consistent improvement in photovoltaic performance, recombination resistance, electron lifetime, and flat-band potential. Future studies using SEM–EDS, Raman spectroscopy, and XRD of powder or thicker annealed films would further confirm the elemental composition and phase structure.

4.2 Band alignment analysis (Mott-Schottky)

The Mott–Schottky (MS) analysis provides valuable insight into the electrochemical properties of the TiO_2-based photoanodes by enabling determination of the flat-band potential (Vfb) and charge carrier density (Nd), which directly influence charge transfer efficiency in quantum dot-sensitized solar cells (QDSCs). The flat-band potential represents the potential at which no space-charge region exists within the semiconductor and serves as an indicator of the conduction band edge position, thereby governing electron injection and transport. It is determined from the linear region of the MS plots using the relation,

$$\frac{1}{C^2} = \frac{2}{\varepsilon \varepsilon_0 c_u N_a} (V - V_{fb})$$

Here, Vfb is obtained by extrapolating the linear region of the $1/C^2$ vs. potential plot to the x-axis. A positive shift in Vfb indicates favorable band-edge realignment and improved interfacial energetics (Wang, X., et al., 2018).

From the x-intercepts of the plots, the Vfb values were found to be −0.747 V for TiO_2, −0.691 V for TiO_2/CdS, and −0.588 V for sulfur-treated TiO_2/CdS (vs Ag/AgCl). The progressive positive shift in Vfb upon CdS sensitization and sulfur treatment indicates favorable modification of interfacial band alignment, consistent with literature reports on surface passivation and dipole-induced band-edge realignment. The carrier density (Nd), calculated from the slope of the MS plots using

$$N_d = \frac{2}{e\epsilon\epsilon_0}\left(\frac{d\left(1/C^2\right)}{dV}\right)^{-1}$$

where e=1.6×10−19e C is the elementary charge, ϵ is the relative permittivity (≈80 for TiO_2 and ≈5.7for CdS), and ϵ0=8.85×10−14F/cm is the permittivity of free space. The term d(1/C2)/dV represents the slope of the Mott-Schottky plot.[16] CdS sensitization leads to an increase in the apparent carrier density, while the reduction in apparent carrier density after sulfur treatment does not indicate poorer conductivity. Instead, it reflects suppression of trap-state charge accumulation at the TiO_2/CdS interface. Sulfur incorporation passivates surface defects that normally store electrons, thereby decreasing the measured capacitance-derived carrier density while simultaneously reducing recombination. Consequently, charge transport becomes more efficient despite the lower apparent Nd (Wang, X., et al., 2018).

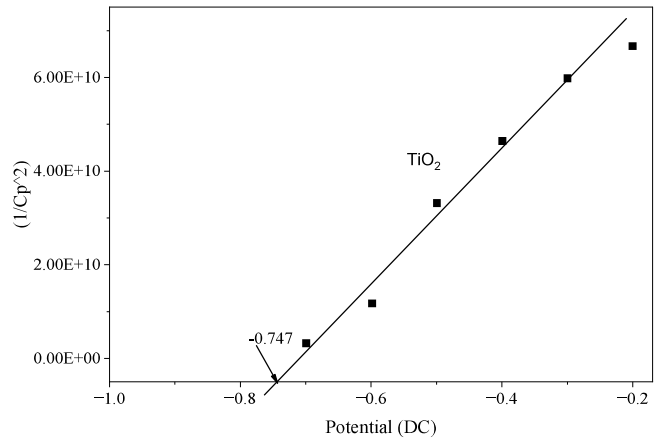

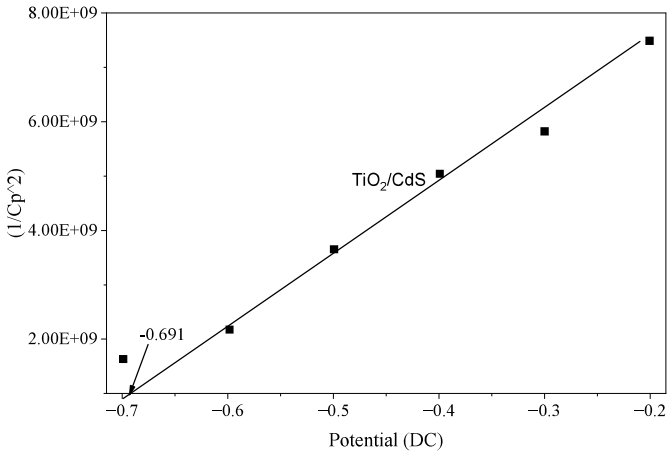

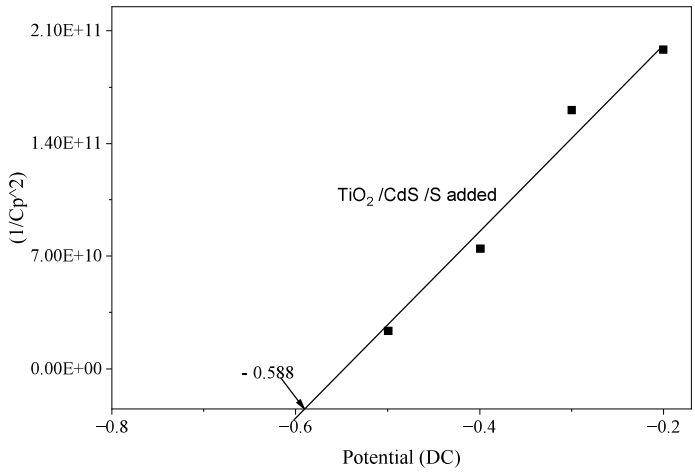

Figure 4: Mott-Schottky ($1/C^2$ vs. Potential) Plots of Bare TiO_2, CdS-Sensitized TiO_2 (TiO_2/CdS), and Sulfur-Doped CdS-Sensitized TiO_2 (TiO_2/CdS-S) Electrodes

Table 2: Flat Band Potentials, Carrier density of TiO_2, TiO_2/CdS, and TiO_2/CdS-S

Sample	Flat band potential (Vfb) (V vs. Ag/AgCl)	Slope ($d(1/C^2)/dV$)) $\times 10^{11}$ ($F^{-2}\wedge V^{-1}$)	Carrier density (N_d) cm^{-3}
TiO_2	-0.747	1.28×10^{11}	1.38×10^{19}
TiO_2 / CdS	-0.691	1.53×10^{10}	1.15×10^{20}
TiO_2/ CdS S	-0.588	5.15×10^{11}	3.42×10^{18}

As shown in Figure 4, the corresponding values summarized in Table 2 were obtained in this research study. Table 2 presents the Mott–Schottky parameters of TiO_2, TiO_2/CdS, and sulfur-treated TiO_2/CdS photoanodes. The flat-band potential shifts positively from −0.747 V for TiO_2 to −0.691 V after CdS sensitization and further to −0.588 V upon sulfur treatment (vs Ag/AgCl), indicating progressive modification of interfacial band alignment. The TiO_2/CdS electrode exhibits the lowest slope (1.53×10^{10} F^{-2} V^{-1}) and the highest apparent carrier density (1.15×10^{20} cm^{-3}), reflecting enhanced electron availability due to CdS sensitization. In contrast, sulfur-treated TiO_2/CdS shows a higher slope (5.15×10^{11} F^{-2} V^{-1}) and reduced carrier density (3.42×10^{18} cm^{-3}), suggesting suppression of trap-assisted charge accumulation and improved interfacial order.

4.3 Charge recombination dynamics (Electrochemical impedance spectroscopy)

Electrochemical impedance spectroscopy (EIS) was employed to evaluate interfacial charge-transfer characteristics and recombination kinetics of the S-doped CdS QD-sensitized photoanodes (S1–S7). The fitted series resistance (Rs) reflects the ohmic contributions from the FTO substrate, contacts, and electrolyte, where a clear minimum is observed for S4 (33.4 Ω) compared to S1 (115 Ω) and S7 (94 Ω), indicating improved electrical pathways and reduced transport losses at the optimized sulphur condition.

The improvement in photovoltaic performance originates from suppression of interfacial trap-assisted recombination. The improvement in EIS and photovoltaic performance suggests that sulfur treatment may reduce interfacial recombination and improve charge transport. However, since direct elemental confirmation was not obtained in this study, this mechanism should be interpreted as a probable explanation based on electrochemical behavior rather than direct structural proof. The charge-transfer/recombination resistance (Rp) increases markedly with sulphur incorporation and reaches the highest value for S4 (216.4 kΩ), followed by S5 (206.6 kΩ) and S3 (188.6 kΩ), while the lowest Rp is obtained for the undoped/least-protected condition S7 (76.2 kΩ). The elevated Rp for S4 suggests strong suppression of interfacial electron back-transfer to the electrolyte, consistent with improved surface passivation and favorable band alignment at the TiO_2/CdS/electrolyte interface.

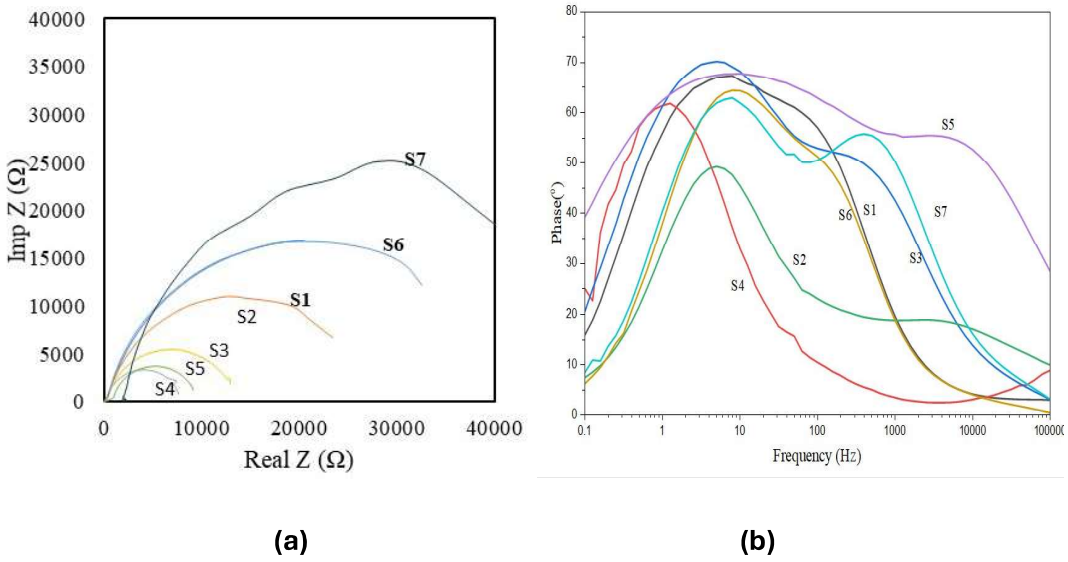

(a) (b)

Figure 5: (a) Impedance spectra characteristics of TiO_2/CdS with varying sulfur (S) mass in Na_2S. (b) Wavelength and Phase of TiO_2/CdS with varying sulfur (S) mass in Na_2S.

Table 3. Parameters of equivalent circuit for different QDSC configuration

	S1	S2	S3	S4	S5	S6	S7
Rs(Ω)	115	62	71.3	33.4	47.4	39	94
Rp(kΩ)	108	166.9	188.57	216.4	206.6	156.1	76.2
CPE	0.524	0.866	0.811	0.713	0.745	0.866	0.898
Peak frequency (Hz)	6.309	5.011	3.981	1.000	1.584	7.943	9.143
Phase (°)	67.216	61.254	69.962	49.293	67.686	64.401	62.942
Electron lifetime	0.0252	0.0317	0.0399	0.1591	0.1004	0.0200	0.0174

Figure 6 illustrates the schematic circuit diagram of the equivalent circuit for a quantum dot-sensitized solar cell. In this model, Rs represents the series resistance, Rp denotes the parallel (shunt) resistance, and CPE corresponds to the constant phase element.

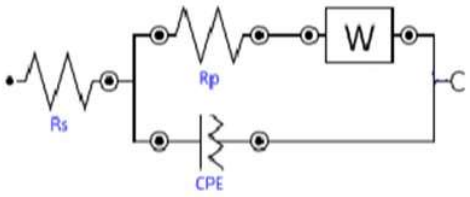

Figure 6: Equivalent circuit

The characteristic recombination frequency derived from Bode analysis further supports this trend. The peak frequency decreases to 1.0 Hz for S4, corresponding to the longest electron lifetime $\tau=1/(2\pi f_{peak})$ of 0.1591 s, whereas higher peak frequencies such as 9.143 Hz (S7) and 7.943 Hz (S6) yield much shorter lifetimes (0.0174 s and 0.0200 s, respectively), indicating accelerated recombination. The constant phase element (CPE) values (0.524–0.898) confirm non-ideal capacitive behavior typical of porous semiconductor electrodes, where deviations from ideality arise from surface roughness, distributed trap states, and interfacial heterogeneity; notably, the lower CPE for S1 (0.524) implies a more heterogeneous interface compared with the more ideal behavior observed for S6–S7 (~0.87–0.90). Overall, the simultaneous reduction in Rs, increase in Rp, and prolonged electron lifetime for S4 demonstrate that the optimized sulphur incorporation effectively enhances charge transport while suppressing recombination, providing an electrochemical basis for the improved photovoltaic output of the corresponding devices.

4.4 Photovoltaic performance (I–V Characteristics of CdS QDSSCs)

Figure 7 and Table 4 illustrate the photovoltaic performance of QDSSCs prepared with different sulfur contents. Significant improvements are observed in sample S4, where voltage increases from 436.7 mV to 470.8 mV (7.8% increase), current density rises from 2.265 mA to 4.176 mA (84.5% increase), and efficiency doubles from 0.262% to 0.519% (98.5% increase), compared to S7 (0 g). These enhancements are attributed to incorporation of sulfur in CdS QDs improving light absorption and facilitating charge transport. However, beyond the optimal sulfur concentration of 0.1410g (e.g., S5 and S6), the performance plateaus or slightly decreases, likely due to excessive sulfur causing aggregation or hindering charge transfer. The lowest current output is observed at 0 g (S7), highlighting the critical role of sulfur in enhancing QDSSC functionality.

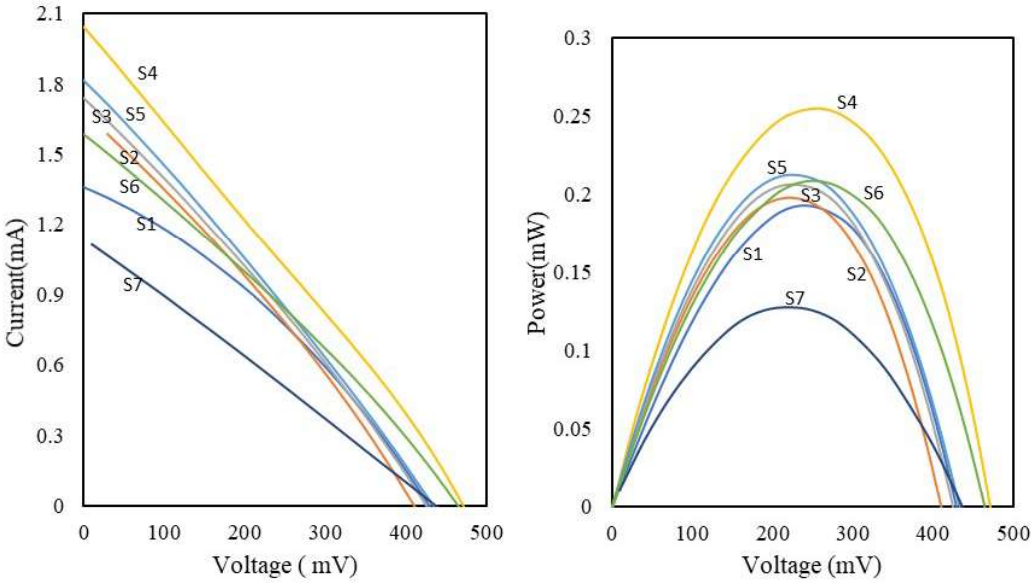

(a) (b)

Figure 7: (a) Current–voltage characteristics of TiO_2/CdS QDSSCs prepared with varying sulfur content (mass listed in Table 1), under simulated AM 1.5G illumination (100 mW cm^{-2}).

(b) Voltage–power characteristics for the same samples

It illustrates that sulfur enhances QDSSC efficiency by improving light absorption, charge transfer, and surface passivation. However, an optimal sulfur concentration (0.1410g) supposed to maximizes efficiency by reducing defects and recombination. At higher concentrations, defects and structural issues may arise, leading to electron trapping leading to lower efficiency. Overall, the results highlight the importance of sulfur-content optimization, with S4 showing the best photovoltaic performance among the investigated samples.

The power-voltage (P-V) graph compares the performance of QDSSCs with varying sulfur (S) concentrations, highlighting the relationship between power output and voltage. Among the samples, the highest power output is achieved at 0.1410g of sulfur (S4), while the lowest is observed at 0 g of sulfur (S7). The peak power for S4 is significantly higher than S7(98.44%), demonstrating the critical role of sulfur in enhancing the solar cell's performance through improved light absorption, charge transfer, and reduced recombination. In contrast, the S7 sample lacks these advantages, resulting in minimal power generation.

Table 4: Photovoltaic Parameters of CdS Quantum Dot-Sensitized Solar Cells

Sample Number	S1	S2	S3	S4	S5	S6	S7
Voltage(mV)	428.6	409.9	424.7	470.8	432.9	464.4	436.7
Current Density (mA m^{-2})	2.781	3.434	3.552	4.176	3.701	3.235	2.265
Fill Factor	33.0	28.7	27.9	26.4	27.0	28.3	26.5
Efficiency (%)	0.394	0.404	0.421	0.519	0.433	0.426	0.262
Maximum Power	0.193	0.198	0.206	0.254	0.212	0.209	0.128

The use of power-voltage plots is essential in QDSSCs as they provide a clear understanding of the cell's efficiency and operating conditions. While current-voltage plots indicate the potential and current capabilities, P-V plots reveal the maximum power point (MPP) the voltage and current at which the solar cell operates most efficiently. This information is crucial for optimizing the design and tuning the parameters to maximize energy output, making the P-V graph a critical tool in evaluating and improving QDSSC performance.

Although the absolute efficiency obtained in this study is lower than highly optimized CdS-based QDSSCs reported in the literature, the present work focuses on the relative improvement caused by controlled sulfur treatment under the same fabrication conditions. The efficiency increased from 0.262% for the untreated/zero-sulfur sample to 0.519% for the optimized S4 sample, corresponding to an approximately 98.5% relative enhancement. Therefore, the significance of the result lies not in achieving record efficiency, but in demonstrating that sulfur availability during SILAR deposition strongly influences recombination dynamics and device output.

4.5 Spectral response (Incident Photon-to-Current Efficiency of QDSSCS)

The Incident Photon-to-Current Efficiency (IPCE) spectra in Figure 8 provide a detailed evaluation of the wavelength-dependent photocurrent generation in TiO_2/CdS Quantum Dot-Sensitized Solar Cells (QDSSCs) with varying sulfur (S) concentrations in CdS QDs. All samples show a decrease in IPCE with increasing wavelength, consistent with the absorption characteristics of CdS quantum dots, which have a bandgap energy of approximately 2.4 eV. This decline reflects the limited absorption and exciton generation at longer wavelengths, highlighting the need for precise quantum dot size control to extend spectral response.

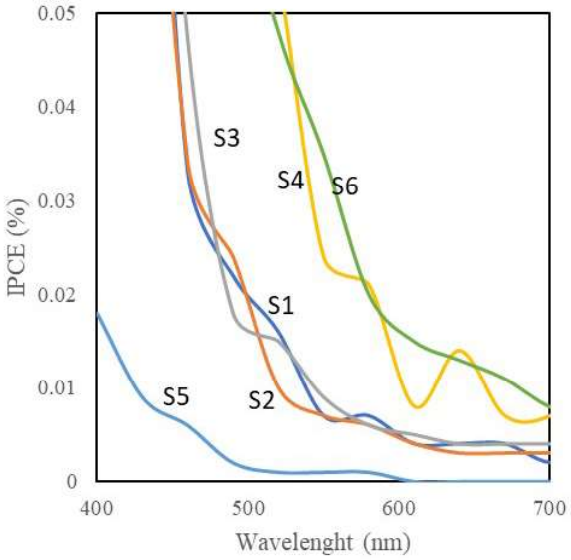

Figure 8: Wavelength vs Photocurrent Efficiency (IPCE) for TiO_2/CdS QDSSCs with the variation of sulfur

Among the different sulfur concentrations, S4 and S6 exhibit pronounced peaks within the 610–670 nm range, suggesting enhanced light-harvesting and efficient charge separation. This can be attributed to an optimal size distribution of CdS quantum dots, promoting efficient photon absorption and electron injection into the TiO_2 conduction band.

The peak in S4, in particular, indicates favorable size quantization effects that align well with the incident light spectrum, maximizing photocurrent generation. This suggests a reduced recombination rate due to improved interfacial energy states and optimized charge transport pathways.

In contrast, S1 and S5 show the lowest IPCE values across all wavelengths, indicating poor light absorption and inefficient charge separation. The absence of significant peaks suggests suboptimal quantum dot growth, possibly due to agglomeration or non-uniform size distribution, leading to increased recombination losses. S2 and S3 display moderate IPCE values with relatively flat spectral profiles, reflecting less effective size quantization and reduced quantum confinement effects. The IPCE measurement in the present study was limited to the 400–700 nm visible region. Extension of the measurement range up to approximately 1100 nm would provide additional information on low-energy photon response and possible defect-related contributions.

These findings underscore the crucial role of sulfur concentration in tuning the optical and electronic properties of CdS quantum dots. The superior performance of S4 demonstrates that precise sulfur content control enhances quantum dot size distribution, leading to improved light absorption and charge carrier dynamics. This emphasizes the importance of strategic quantum dot engineering for optimizing the photovoltaic performance of TiO_2/CdS QDSSCs.

CONCLUSION

Controlled sulfur addition during the SILAR deposition process influenced the photovoltaic and electrochemical performance of TiO_2/CdS quantum dot-sensitized solar cells. The optimized sample showed an efficiency improvement from 0.262% to 0.519%, together with increased photocurrent, higher open-circuit voltage, greater recombination resistance, and longer electron lifetime. These results suggest that sulfur treatment may suppress interfacial recombination and improve charge transport within the TiO_2/CdS photoanode system.

However, SEM, XRD, and FTIR analyses did not provide conclusive evidence for CdS crystallinity or sulfur incorporation because the structural and spectroscopic differences among the samples were relatively small. The CdS phase may be amorphous or poorly crystalline, possibly due to insufficient annealing temperature. Therefore, further characterization using SEM–EDS, Raman spectroscopy, and XRD analysis of powder or thicker annealed films is required to confirm elemental composition and phase formation.

Overall, the electrochemical and photovoltaic results indicate that controlled sulfur treatment is a promising approach for improving TiO_2/CdS QDSSC performance, although further structural confirmation is necessary to fully validate the proposed mechanism.

REFERENCES

[1] Grätzel, M. (2001). Dye-sensitized solar cells. *Journal of Photochemistry and Photobiology C: Photochemistry Reviews, 4*(2), 145-153.

[2] Nozik, A. J. (2002). Quantum dot solar cells. *Physica E: Low-dimensional Systems and Nanostructures, 14*(1-2), 115-120.

[3] Klimov, V. I. (2006). Detailed-balance power conversion limits of nanocrystal quantum dot solar cells. *Applied Physics Letters, 89*(12), 123118.

[4] Shockley, W., & Queisser, H. J. (1961). Detailed balance limit of efficiency of p-n junction solar cells. *Journal of Applied Physics, 32*(3), 510-519.

[5] O'Regan, B., & Grätzel, M. (1991). A low-cost, high-efficiency solar cell based on dye-sensitized colloidal TiO_2 films. *Nature, 353*(6346), 737-740.

[6] Wang, P., Zakeeruddin, S. M., Moser, J. E., Humphry-Baker, R., & Grätzel, M. (2003). A stable quasi-solid-state dye-sensitized solar cell with an amphiphilic ruthenium sensitizer and polymer gel electrolyte. *Nature Materials, 2*(6), 402-407.

[7] Bisquert, J., Cahen, D., Hodes, G., Rühle, S., & Zaban, A. (2004). Physical chemical principles of photovoltaic conversion with nanoparticulate, mesoporous dye-sensitized solar cells. *Journal of Physical Chemistry B, 108*(24), 8106-8118.

[8] Chen, X., & Mao, S. S. (2007). Titanium dioxide nanomaterials: Synthesis, properties, modifications, and applications. *Chemical Reviews, 107*(7), 2891-2959.

[9] Kamat, P. V. (2008). Quantum dot solar cells: Semiconductor nanocrystals as light harvesters. *Journal of Physical Chemistry C, 112*(48), 18737-18753.

[10] Hodes, G. (2008). Comparison of dye- and semiconductor-sensitized porous nanocrystalline liquid junction solar cells. *Journal of Physical Chemistry C, 112*(46), 17778-17787.

[11] Lee, H. J., Yum, J. H., Moon, S. J., et al. (2009). CdS quantum dot-sensitized solar cells exceeding 4% efficiency employing an organic hole conductor. *Journal of Physical Chemistry C, 113*(46), 19921-19927.

[12] Santra, P. K., & Kamat, P. V. (2012). Mn-doped quantum dot sensitized solar cells: A strategy to boost efficiency over 5%. *Journal of the American Chemical Society, 134*(50), 2508-2514.

[13] Lu, H., Tian, J., Cao, G., et al. (2014). Sulfur-doped TiO_2 nanoparticles for photoelectrochemical water splitting. *Journal of Physical Chemistry C, 118*(47), 25329-25337.

[14] Li, W., Ding, H., Ji, H., Dai, W., Guo, J., & Du, G. (2018). Photocatalytic degradation of tetracycline hydrochloride via a CdS-TiO2 heterostructure composite under visible light irradiation. Nanomaterials, 8(6), 415.

[15] Wang, X. et al. (2018) – "Enhanced Photoelectrochemical Performance of CdS Quantum Dot-Sensitized TiO_2." *Journal of Solar Energy Materials*.

[16] Zhang, Y. et al. (2017) – "Charge Transfer in CdS-Sensitized TiO_2 Nanostructures." *ACS Applied Materials & Interfaces*.

[17] Kunnamareddy, M., Rajendran, R., Sivagnanam, M., Rajendran, R., & Diravidamani, B. (2021). Nickel and sulfur codoped TiO 2 nanoparticles for efficient visible light photocatalytic activity. *Journal of Inorganic and Organometallic Polymers and Materials*, *31*, 2615-2626.

[18] O'Hayre, R., Nanu, M., Schoonman, J., & Goossens, A. (2007). Mott− Schottky and charge-transport analysis of nanoporous titanium dioxide films in air. The Journal of Physical Chemistry C, 111(12), 4809-4814.

[19] Zhu, Q., Wang, J., Chen, S., Fu, H., Zhang, J., Gao, H., & Liao, Y. (2022). Effect of the organic sulfur source on the photocatalytic activity of CdS. *RSC advances*, *12*(18), 11262-11271.

[20] Chen, Y., Qin, Z., Chen, T., Su, J., Feng, X., & Liu, M. (2016). Optimization of $(Cu_2Sn)_xZn_{3(1-x)}S_3$/CdS pn junction photoelectrodes for solar water reduction.